Front. Eng. Manag. 2024, 11(1): 92–106
https://doi.org/10.1007/s42524-023-0285-x

RESEARCH ARTICLE

Haoran LI, Yunpeng LU, Yaqiu LI, Junyi ZHANG

A dynamic speed guidance method at on-ramp merging areas of urban expressway considering driving styles

Abstract Dynamic speed guidance for vehicles in on-ramp merging zones is instrumental in alleviating traffic congestion on urban expressways. To enhance compliance with recommended speeds, the development of a dynamic speed-guidance mechanism that accounts for heterogeneity in human driving styles is pivotal. Utilizing intelligent connected technologies that provide real-time vehicular data in these merging locales, this study proposes such a guidance system. Initially, we integrate a multi-agent consensus algorithm into a multi-vehicle framework operating on both the mainline and the ramp, thereby facilitating harmonized speed and spacing strategies. Subsequently, we conduct an analysis of the behavioral traits inherent to drivers of varied styles to refine speed planning in a more efficient and reliable manner. Lastly, we investigate a closed-loop feedback approach for speed guidance that incorporates the driver's execution rate, thereby enabling dynamic recalibration of advised speeds and ensuring fluid vehicular integration into the mainline. Empirical results substantiate that a dynamic speed guidance system incorporating driving styles offers effective support for human drivers in seamless mainline merging.

Keywords driving styles, speed guidance, driving safety assistance, on-ramp merging

Received Aug. 5, 2023; revised Sep. 15, 2023; accepted Sep. 25, 2023

Haoran LI
School of Automobile and Traffic Engineering, Wuhan University of Science and Technology, Wuhan 430065, China; Suzhou Automotive Research Institute, Tsinghua University, Suzhou 215134, China

Yunpeng LU
School of Automobile and Traffic Engineering, Wuhan University of Science and Technology, Wuhan 430065, China

Yaqiu LI
School of Transportation, Southeast University, Nanjing 211189, China; Graduate School of Advanced Science and Engineering, Hiroshima University, Higashi Hiroshima 739-8529, Japan

Junyi ZHANG (✉)
School of Transportation, Southeast University, Nanjing 211189, China
E-mail: zjy890321@seu.edu.cn

This research was supported by National Start-up Research Fund at Southeast University (Grant No. 5721002303), Science and Technology Program of Suzhou (Grant No. SYC2022078), Natural Science Foundation of Jiangsu Province (Grant No. BK20220243), China Postdoctoral Science Foundation (Grant No. 2023M742033), and Key R&D Program Projects of Hubei Province (Grant No. 2023DJC195).

1 Introduction

Currently, the automotive industry is witnessing a pronounced shift towards electrification and enhanced intelligence. Electrification is a potent means of curtailing carbon emissions and safeguarding the environment (Kennedy and Philbin, 2019). The emergence of Connected and Autonomous Vehicle (CAV) technologies has been pivotal for reducing and preventing vehicular collisions, bolstering traffic safety, and optimizing transportation efficiency (Gao et al., 2023). Nevertheless, the attainment of these objectives remains a formidable challenge, primarily because of the continued presence of Human-driven Vehicles (HVs) on roadways. The coexistence of HVs introduces complexity, particularly concerning the intricate tasks of speed regulation and safe merging with other vehicles. Merging entails a multi-faceted endeavor that requires interactions with multiple vehicles to establish a secure and suitable gap. In the current landscape, the advancement towards smart cities mandates the establishment of an autonomous and interconnected infrastructure (Chen, 2019), offering an avenue to address longstanding urban traffic challenges. A pragmatic and effective approach involves implementing a central controller within this connected and autonomous framework. This central controller can harness vehicle state data to steer vehicle speeds and facilitate secure merging.

Urban expressways host numerous ramp intersections. The disparity in speeds between vehicles traversing the main thoroughfare and those entering the ramp renders

these intersections high-risk zones for potential accidents. Conventionally, vehicles on an on-ramp exhibit slower speeds than their counterparts on the mainline. To ensure secure and stable merging, the optimization and adjustment of these vehicle speeds have emerged as paramount considerations.

In scenarios where both HVs and CAVs coexist, the merging of vehicles is necessary owing to the influence of human factors. Decisions regarding risk in this collaborative human–machine setting are inherently intricate. One possible approach is to provide some guidance on the speed of HVs. Existing research on vehicle-merging strategies has predominantly focused on cooperative control and decision-making among multiple vehicles, with relatively limited attention paid to human factors. This study addresses the merging strategy by integrating human factors into vehicle merging approaches in situations that include both HVs and CAVs on the road. The cooperative strategy proposed in this study accommodates variances in driving styles among drivers, thereby realizing distinct speed guidance strategies.

2 Literature review

2.1 Existing efforts

Numerous algorithms rooted in heuristics and optimization principles have emerged to address the intricate challenges associated with merging on highway ramps (Rios-Torres and Malikopoulos, 2017). The heuristic approach employs virtual platooning to align ramp vehicles with the mainline. By accounting for the longitudinal distance between each vehicle and the merging point, longitudinal vehicle control can be implemented effectively (Uno et al., 1999). However, given the independent movement of each vehicle, enhancing overall traffic efficiency on the road poses a formidable challenge.

Building on Uno et al. (1999)'s groundwork, other methodologies have evolved, culminating in the development of a real-time ramp intersection vehicle merging control algorithm (Lu et al., 2004). This innovative approach leverages a local control station to offer traffic recommendations to vehicles at ramp entrances. Information is seamlessly disseminated to individual vehicles via vehicle-to-infrastructure (V2I) communication, and a fuzzy controller is deployed to fine-tune vehicle speeds. This strategy significantly augments traffic efficiency at ramp intersections (Milanés et al., 2011).

A noteworthy contribution in this domain involves the introduction of a method for multivehicle coordinated ramp merging. This method empowers roadside units to ascertain the optimal timing for ramp vehicle merging, while proactively creating gaps to accommodate these vehicles (Marinescu et al., 2012). Rios-Torres and Malikopoulos (2017) summarized relevant studies on vehicle merging on highway on-ramps.

While controllers grounded in Reinforcement Learning (RL) have encountered challenges in meeting safety requirements, a promising avenue is the utilization of RL to make vehicle merging decisions, coupled with the adoption of Model Predictive Control for vehicle control (Kimura et al., 2022). This approach harmoniously integrates decision-making and control processes.

In a departure from conventional cooperative algorithms, a noncooperative framework premised on dynamic games acknowledges the competitive dynamics between mainline vehicles and ramp vehicles (Ladino and Wang, 2020). This novel approach offers new insights into merging landscapes.

V2I communication plays a pivotal role in merging CAVs on ramps by transmitting vehicle information to the central controller. This controller effectively groups vehicles and determines the optimal merging sequence by applying the shortest path planning algorithm. Such an approach holds the promise of reducing fuel consumption during vehicle merging and enhancing overall traffic efficiency (Shi et al., 2021).

Numerous approaches have been proposed for single-vehicle speed guidance systems, including methods such as the augmented Hamiltonian and Sequential Quadratic Programming approach (Chen et al., 2022), and the fusion of the green wave concept with the speed guidance model (HomChaudhuri et al., 2017; Xu et al., 2020). Moreover, studies have explored the integration of car-following models (Liang et al., 2018), delineation of state constraints, and derivation of real-time speed distribution maps with energy consumption as the optimization objective (Han et al., 2018). These endeavors share the common goal of curbing energy consumption, averting collisions, and optimizing both position and speed without extending the travel time.

Furthermore, a pioneering intersection vehicle motion model has emerged, affording drivers the capacity to select the most favorable driving path and speed (Zhao et al., 2020). However, it is imperative to note that these studies are centered on the speed guidance of individual vehicles. To address the specific context of speed guidance in the merging area of ramps, a coordinated control approach for multiple vehicles is imperative.

Numerous multivehicle speed guidance methodologies have emerged to enhance traffic performance. One approach entails the application of a mixed-integer linear programming (MILP) model to categorize vehicles into groups and orchestrate their traversal of intersections at predetermined speeds (Wu et al., 2015; Yu et al., 2018). Another method centers on the development of a variable-speed limit controller capable of collaborating with a ramp metering controller to significantly enhance traffic efficiency (Zhang and Ioannou, 2017). Furthermore, an adaptive control strategy has been introduced, where continuous control variables undergo adjustment based

on inputs, such as traffic speed and density, steered by a Deep RL algorithm (Cheng et al., 2022). This study unequivocally underscores the efficacy of guiding or constraining vehicle speeds to augment traffic efficiency within merging zones.

Moreover, a co-ecological driving model rooted in platooning principles has shown that the amalgamation of autonomous and conventional vehicles can effectively reduce fuel consumption (Zhao et al., 2018). To realize fuel reduction objectives, the incorporation of traffic state information is of paramount significance. Previous research seamlessly integrated traffic state prediction, ecological driving speed control, and powertrain management to craft an ecological driving system that exhibits resilience across diverse traffic scenarios (Huang et al., 2018). These studies underscored the pivotal role of integrating traffic state information and adhering to ecological driving principles in the pursuit of fuel efficiency and overall system optimization.

In addition, Ci et al. (2019) delved into the integration of V2I communication into the speed guidance system at signalized intersections. Furthermore, multiple speed guidance models have been devised, each tailored to specific optimization objectives and variables, as demonstrated in the research by Han et al. (2018) and Fang et al. (2020). It is noteworthy that this study places a significant emphasis on accommodating individual driving styles within the model.

Currently, two primary paradigms dominate multivehicle cooperative control: One involves optimizing the speed distribution of all vehicles while treating vehicle–vehicle interaction as a constraint, and the other focuses on optimizing the speed profiles of lead and following vehicles through vehicle platooning techniques. However, these methods present notable complexities and time-consuming aspects for practical engineering applications. To address these challenges, a simplified approach based on an intelligent driver model has been proposed (Xin et al., 2018). Previous studies formulated optimization models for determining the optimal vehicle acceleration and deceleration based on fuel consumption comparisons (Chen et al., 2015). Additionally, a Model Predictive Control framework was instituted to execute longitudinal control while considering the uncertainties associated with autonomous driving (Zhao and Zhang, 2021). Nonetheless, it is imperative to acknowledge that, while enhancing speed control efficiency, these methods may overlook crucial factors linked to driving styles, which can exert a substantial influence on drivers' confidence levels.

2.2 Research gap

The aforementioned speed guidance and multivehicle cooperative control techniques prove beneficial in enhancing road traffic efficiency. However, it is worth noting that these approaches often overlook the crucial influence of human factors. Some of these methods find application solely in environments dominated by CAVs, rendering them less effective when HVs coexist with CAVs, particularly on ramps where both types of vehicles converge. To address this challenge, certain studies have ventured into the realm of merging CAVs and HVs in ramp areas.

One approach involves categorizing vehicle-merging scenarios into distinct categories, including scenarios involving only CAVs or a mix of CAVs and HVs. Subsequently, merging strategies are tailored accordingly (Karimi et al., 2020). Another method leverages Neural Networks to formulate a predictive model for the merging intentions of drivers. By collecting data through roadside units, including HVs' speeds in the ramp area, and employing Neural Network models, these studies predict the likelihood of HVs merging and facilitate a seamless convergence of CAVs and HVs at the merging juncture (Kherroubi et al., 2022). However, it is noteworthy that these studies have not considered the diverse driving styles exhibited by HVs.

Numerous investigations have focused on driving styles using both subjective and objective measurements. These studies have led to the integration of driving characteristics into driving-assistance systems. For instance, Miyajima et al. (2007) harnessed naturalistic driving data to formulate a relative speed and distance model, shedding light on the car-following behavior. Several models have factored in elements such as safety distance, obstacle positioning, and turning intentions to establish an intricate relationship between vehicle motion and driving styles (Gipps, 1986; Moridpour et al., 2012). Additionally, prior research has scrutinized drivers' response characteristics and vehicle dynamics during collision conflicts using Monte Carlo simulations (Kim and Jeong, 2014). The attributes of bounded rationality inherent in drivers have been analyzed for their implications on speed guidance (Tang et al., 2017). Furthermore, a study introduced a cooperative platoon control method within a traffic scenario characterized by the coexistence of CAVs and HVs (Gong and Du, 2018). However, it is worth noting that limited research has explored the influence of driving style characteristics on drivers' compliance with speed guidance.

An effective speed guidance strategy should also prioritize passenger comfort. Excessive acceleration and deceleration can significantly affect passenger comfort levels. By incorporating the minimization of acceleration, jerk, and jerk derivatives into the calculation of the optimal merging trajectory, abrupt changes in the vehicle speed during the merging process can be mitigated to enhance driving comfort (Ntousakis et al., 2016). This study, notably, considers factors in various driving styles, as reflected in the maximum acceleration constraints, thereby enhancing the adaptability of the speed guidance

method. Consequently, passenger comfort improves, leading to an elevated level of comfort that can foster greater driver compliance.

2.3 Research purpose

In this study, we present a dynamic speed guidance approach tailored for merging vehicles on urban expressways, considering various driving styles. First, we employ a multi-agent consensus algorithm to orchestrate a harmonized speed and distance profile for vehicles on both the mainline and on-ramp, thereby ensuring a cohesive merging process. Second, we examine driving behavior characteristics, discerning distinctions among drivers with diverse styles, and leveraging this insight to optimize pre-planned speeds. Finally, we explore a closed-loop feedback speed guidance method that allows for real-time adjustments of the guided speeds according to the driver's specific style. This comprehensive approach facilitates seamless merging of vehicles within the merging area, fostering uninterrupted traffic flow and optimizing the confluence process efficiently.

3 Framework of the speed guidance system at the on-ramp merging areas

3.1 Speed guidance scenario at the on-ramp merging areas

On-ramp merging areas frequently act as bottlenecks for urban road traffic. The implementation of appropriate speed-guidance measures has the potential to alleviate traffic congestion and enhance the overall efficiency of road traffic. This ensures that drivers can afford ample space and response time to adjust their speeds adeptly. Vehicle-to-everything (V2X) technology assumes a pivotal role in this context by facilitating vehicle communication, which in turn enables speed guidance through the reception of information from roadside equipment and vehicle communication devices. This technological underpinning significantly augments the efficacy of speed control and contributes to the amelioration of traffic flow within the on-ramp merging areas.

This section describes the development of a speed guidance methodology meticulously tailored for the on-ramp merging area, as illustrated in Fig. 1. The primary objective of this method is to provide drivers with the recommended merging speeds as they transition to the mainline. It should be noted that the method in this paper is based on the following assumptions:

(1) This study excluded considerations related to pedestrians and non-motor vehicles.

(2) It focuses on a merging area characterized by a single lane.

(3) Vehicles engage in longitudinal merging without lateral movements.

Based on these assumptions, the speed guidance method for vehicles within on-ramp merging areas, cognizant of consensus dynamics and driving styles, unfolds across three primary stages:

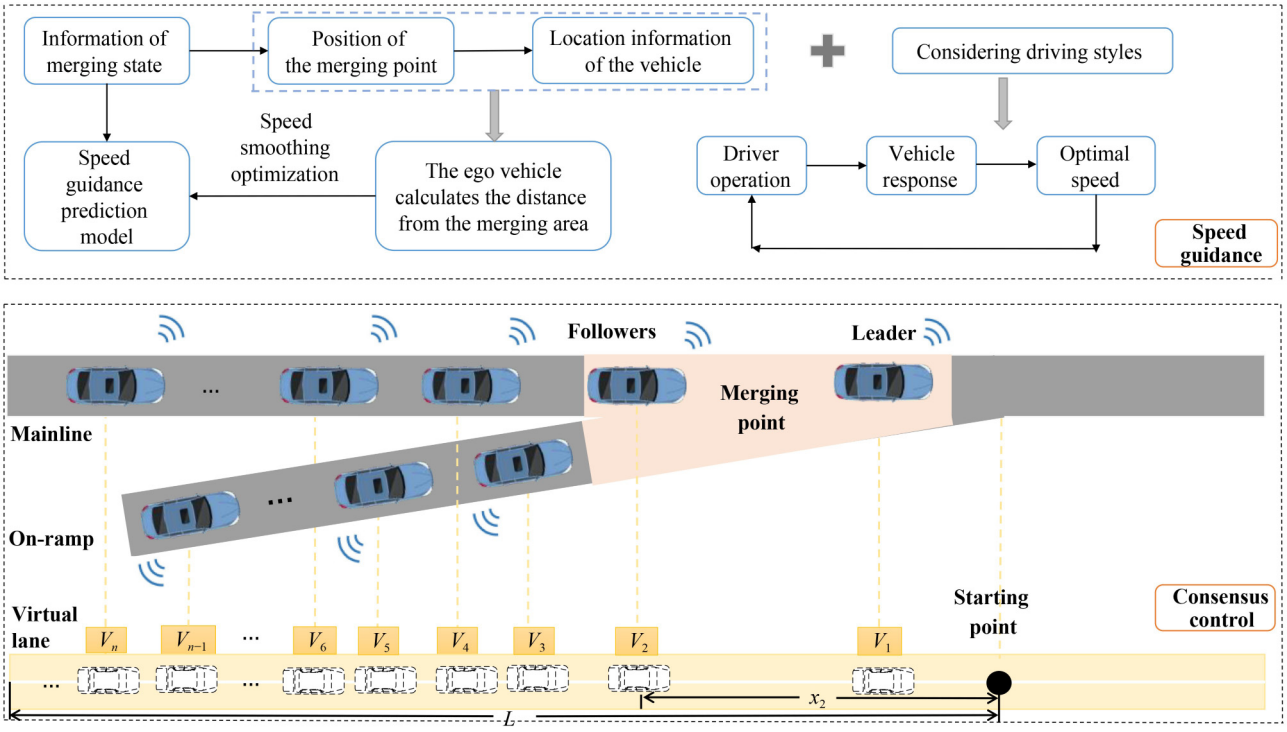

Fig. 1 Framework of the speed guidance system.

(1) In the initial stage, V2X technology is used to enable vehicles in the merging zone to receive state information from the leading vehicle and the preceding vehicle.

(2) In the second stage, a central controller computes the optimal guidance speed by judiciously assimilating the merging state information and integrating vehicle-related data pertinent to consensus dynamics and driving styles.

(3) Finally, the third stage orchestrates the dynamic adjustment of vehicle speeds in response to real-time fluctuations in the merging environment.

3.2 Development of a traffic prediction model

In accordance with the prevailing traffic conditions within the merging area, including factors such as vehicle volume, speed, merging time (t_{reach} or t_g), and precise positions of vehicles, on-ramp vehicles can systematically compute their respective distances from the merging point (d_{int}) using their positional information. This calculation depends on the estimation of the time required to reach the merging point (t_{reach}) under the assumption that the vehicle maintains its present speed (v_0).

$$t_{\text{reach}} = \frac{d_{\text{int}}}{v_0}. \tag{1}$$

At a given time t_{reach}, if the number of vehicles on the mainline remains consistently low and stable, these vehicles have the capacity to maintain a constant speed. Conversely, when the number of vehicles on the mainline fluctuates and increases significantly, an evaluation of the current traffic state within the merging area is necessary. When the traffic flow on the mainline is heavy, it is necessary to assess whether it is possible to pass through the merging area by slowing down the ramp vehicles without stopping and waiting. Conversely, when the traffic volume is relatively low, on-ramp vehicles must assess whether they can accelerate sufficiently to traverse the merging point within the designated merging time t_g, utilizing their maximum acceleration $a_{\max}$ and road maximum speed limit $v_{\lim}$. The travel distance of a vehicle within a given time can be computed using Eq. (2), and on-ramp vehicles can determine the feasibility of accelerating through the merging point without halting based on the conditions outlined in Eq. (3). If Eq. (3) holds true, on-ramp vehicles can execute acceleration through the merging point without stopping; otherwise, they must determine whether they can navigate the merging point by decelerating. t_g represents the time window for ramp vehicles to pass, during which the mainline vehicles have not yet reached the merging point and ramp vehicles can accelerate through. t_g' represents the waiting time, during which the mainline vehicles are passing through the merging point and ramp vehicles need to consider slowing down to reach the merging area to avoid stopping and waiting. $v_{\lim}$ and $v_{\lim}'$ represent the maximum and minimum speed limits on the ramp, respectively.

$$d = \begin{cases} v_0 t_g + \dfrac{1}{2} a_{\max} t_g^2 & \dfrac{v_{\lim} - v_0}{a_{\max}} \geqslant t_g \\ \dfrac{v_{\lim}^2 - v_0^2}{2a_{\max}} + v_{\lim}\left(t_g - \dfrac{v_{\lim} - v_0}{a_{\max}}\right) & \dfrac{v_{\lim} - v_0}{a_{\max}} < t_g \end{cases}, \tag{2}$$

$$d > d_{\text{int}}. \tag{3}$$

Subsequently, the on-ramp vehicle proceeds to evaluate whether it has the capability to decelerate and navigate through the merging point without the necessity of coming to a complete stop. To facilitate this determination, the distance covered by the vehicle during the remaining time t_g' of the second merging opportunity is computed using Eq. (4). This computation incorporates the maximum reduction acceleration $a_{\min}$, while ensuring that the resultant minimum speed does not fall below the prescribed road speed limit $v_{\lim}'$. In the event that Eq. (5) is fulfilled, signifying that the conditions outlined therein are satisfied, the on-ramp vehicle can effectively traverse the merging point without the need to halt its progression. However, if the calculated distance d does not satisfy Eq. (5), the vehicle can only stop at the merging point and wait to merge.

$$d = \begin{cases} v_0 t_g + \dfrac{1}{2} a_{\min} t_g'^2 & \dfrac{v_{\lim}' - v_0}{a_{\min}} \geqslant t_g' \\ \dfrac{v_{\lim}^2 - v_0^2}{2a_{\min}} + v_{\lim}'\left(t_g' - \dfrac{v_{\lim} - v_0}{a_{\min}}\right) & \dfrac{v_{\lim}' - v_0}{a_{\min}} < t_g' \end{cases}, \tag{4}$$

$$d < d_{\text{int}}. \tag{5}$$

3.3 Optimization of guidance acceleration and deceleration

In pursuit of the twin objectives of fostering seamless traffic flow and enhancing fuel efficiency in the context of on-ramp merging, this study introduced a trigonometric function optimization approach for acceleration and deceleration. This method is adept at generating smooth speed profiles characterized by continuous acceleration, as shown in Eq. (6). This feature is enabled by utilizing the traffic prediction model established in the preceding section, which empowers on-ramp vehicles to execute seamless deceleration or acceleration maneuvers as they traverse the merging point.

$$v_{\text{opt}}(t) = \begin{cases} v_a - v_d \cos(\omega t) & 0 \leqslant t < \dfrac{\pi}{2\omega} \\ v_a - v_d \dfrac{\omega}{\varphi} \cos\varphi\left(t - \dfrac{\pi}{2\omega} + \dfrac{\pi}{2\varphi}\right) & \dfrac{\pi}{2\omega} \leqslant t < \dfrac{\pi}{2\omega} + \dfrac{\pi}{2\varphi}, \\ v_a + v_d \dfrac{\omega}{\varphi} & \dfrac{\pi}{2\omega} + \dfrac{\pi}{2\varphi} \leqslant t \leqslant t_f \end{cases} \tag{6}$$

where v_a is the average target speed of the vehicle, and t_f is the total time:

$$t_f = \begin{cases} t_g & \text{if acceleration} \\ t'_g & \text{if deceleration} \end{cases}. \tag{7}$$

By leveraging the foundation provided by the traffic prediction model detailed earlier, on-ramp vehicles can execute smooth transitions through the merging point by either accelerating or decelerating. To facilitate this quest for smooth and efficient speed guidance, we employed a trigonometric function optimization method, drawing inspiration from the work of Barth et al. (2011). As depicted in Eq. (6), this method yields speed profiles characterized by a seamless and continuous acceleration trajectory during the speed optimization process.

To reduce fuel consumption, the vehicle does not need to stop through the merging point during the merging process, and v_a is given by Eq. (8):

$$v_a = \begin{cases} \dfrac{d_{\text{int}}}{t_g} & \text{if acceleration} \\ \dfrac{d_{\text{int}}}{t'_g} & \text{if deceleration} \end{cases}. \tag{8}$$

v_d represents the difference between the average target vehicle speed and current vehicle speed v_0, as shown in Eq. (9):

$$v_d = v_a - v_0. \tag{9}$$

Two parameters in Eq. (6), i.e., ω and φ, determine the shape of the vehicle speed-guide profile. According to the research of Barth et al. (2011), the larger the ω is, the less energy consumption of the speed guidance curve will be, as shown below.

$$\omega = \max\{\omega\}. \tag{10}$$

For driver comfort, the maximum rate of acceleration and acceleration change should not be too large, and the following conditions should be satisfied (Barth et al., 2011), where $|J|$ is the smoothness coefficient, representing the constraint relationship among v_d, ω, and φ.

$$|a_{\max}| \leqslant 2.5 \text{ m/s}^2, \tag{11}$$

$$|J| = |v_d \omega \varphi| \leqslant 10. \tag{12}$$

The target vehicle speed v should meet the distance constraint:

$$d_{\text{int}} = \int_0^{t_f} v \mathrm{d}t. \tag{13}$$

Combine all equations above to obtain the constraint Eq. (14):

$$\begin{cases} d_{\text{int}} = \displaystyle\int_0^{\frac{\pi}{2\omega}} (v_a - v_d \cos(\omega t)) \mathrm{d}t \\ \qquad + \displaystyle\int_{\frac{\pi}{2\omega}}^{\frac{\pi}{2\omega}+\frac{\pi}{2\varphi}} \left(v_a - v_d \frac{\omega}{\varphi} \cos\varphi \left(t - \frac{\pi}{2\omega} + \frac{\pi}{2\varphi} \right) \right) \mathrm{d}t \\ \qquad + \left(v_a + v_d \dfrac{\omega}{\varphi} \right) \left(\dfrac{d_{\text{int}}}{v_a} - \dfrac{\pi}{2\omega} - \dfrac{\pi}{2\varphi} \right) \\ |J| = |v_d \omega \varphi| \leqslant 10 \\ |a_{\max}| \leqslant 2.5 \\ \varphi = \max\{\varphi\} \end{cases}. \tag{14}$$

4 The speed optimization method

4.1 Consensus

Vehicles within the merging area can be viewed as a modification of the conventional vehicle platoon, which typically consists of two or more vehicles traveling in a single lane at a predetermined distance and speed. In contrast to the conventional platoon, the merging area platoon encompasses vehicles originating from both the main lane and on-ramp. This platoon configuration can be conceptualized as a dynamic network system, wherein the platoon vehicles assume the role of nodes, whereas the exchange of information among them constitutes the edges. This interaction gives rise to a graph-based topology that facilitates seamless communication among vehicles within the platoon. A platoon communication topology with N vehicles can be modeled as a directed graph $G_N = (V_N, E_N, A_N)$, which includes a set of nodes $V_N = \{1, ..., N\}$, a set of edges $E_N \subseteq V_N \times V_N$, and a weighted adjacency matrix $A_N = [a_{N,ij}]_{N \times N}$.

Within the merging area, a platoon comprising N vehicles is established, and its composition is determined based on the relative spacing between the vehicles. By utilizing vehicle-mounted inertial navigation and GPS systems, each vehicle within the platoon acquires precise data pertaining to its absolute position, speed, and coordinated universal time. As exemplified in Fig. 2, within the peer-to-leader-follower communication topology, a vehicle has the capacity to receive comprehensive motion state information from both the lead vehicle and the preceding vehicles. This dataset includes critical parameters such as the absolute position, speed, and acceleration.

The vehicle platoon system can be regarded as a dynamic network, wherein the platoon vehicles serve as dynamic network nodes and the links facilitating information exchange between vehicles represent the edges within this dynamic network. The node dynamics model, in this context, adopts a third-order linear model to characterize the longitudinal dynamics of the vehicle. This model can be expressed succinctly as follows:

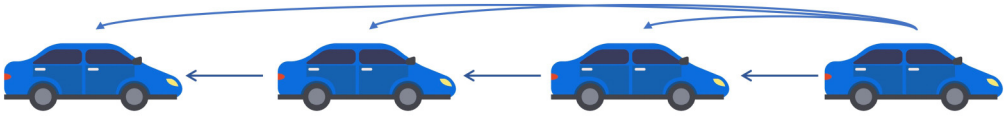

Fig. 2 Predecessor-leader following.

$$\begin{cases} \dot{x}_i(t) = v_i(t) \\ \dot{v}_i(t) = a_i(t) \\ \dot{a}_i(t) = -\dfrac{1}{T_i}a_i(t) + \dfrac{1}{T_i}u_i(t) \end{cases}, \tag{15}$$

where $x_i(t)$, $v_i(t)$, and $a_i(t)$ represent the position, speed, and acceleration of vehicles at time t, respectively. $i = 0, 1, \ldots$ represents the number of each vehicle in the platoon, where $i = 0$ represents the leader vehicle. $u_i(t)$ is the control input of vehicles at time t, and T_i is the time constant of the transmission system.

Within the cooperative merging guidance system designed for vehicle platoons, the leader vehicle assumes the pivotal role of being the foremost vehicle in traversing the merging point, adhering to the optimal traffic order meticulously determined by the system. Typically, the leader vehicle operates at the desired speed. However, when the initial speed of the leader vehicle deviates from the desired speed, a virtual leader vehicle can be introduced. The virtual leader vehicle mirrors the desired speed while starting from the same initial position as the actual leader vehicle.

To ensure the seamless and secure merging of vehicles within the platoon, it is imperative to uphold a consensus among its members. This consensus, or unanimity, within the platoon entails the following key considerations.

$$\begin{cases} \lim\limits_{t\to\infty} \|v_i(t) - v_0(t)\| = 0 \\ \lim\limits_{t\to\infty} \|x_i(t) - x_0(t)\| = r_{i0}^* \end{cases}, \tag{16}$$

where r_{i0}^* represents the distance between the vehicle i and the leader vehicle, which is a constant value.

To attain the overarching consensus objective within the vehicle platoon, individual vehicles are capable of receiving essential state information (position, speed, and acceleration) and timestamp t from their fellow platoon members. By integrating the advanced distributed consensus protocol proposed in this study, the control input for platoon vehicles can be effectively computed, thus aligning with the collective objective of the vehicle platoon.

The consensus control protocol governing the behavior of vehicles within the queue is outlined as follows:

$$u_i(t) = \frac{1}{d_i}\sum_{j=0}^{N}\alpha_{ij}(k_{ij}(x_j(t-\tau_{ij}(t)) - x_i(t) + v_0(t-\tau_{i0}(t))\tau_{ij}(t) - r_{ij}) + b_{ij}(v_j(t-\tau_{ij}(t)) - v_i(t)) + a_{ij}(t-\tau_{ij}(t))), \tag{17}$$

where a_{ij} denotes the adjacency matrix element. The adjacency matrix signifies the connections between a vehicle and the rest of the vehicles in the platoon. k_{ij} and b_{ij} denote the adjustment parameter, r_{ij} represents the distance between vehicles i and j, $d_i = \sum_{j=0}^{N}\alpha_{ij}$ denotes the vehicle degree, and $\tau_{ij}(t)$ and $\tau_{i0}(t)$ represent the communication delays of vehicle j and the leader vehicle sending information to vehicle i. Because platoon vehicles are typically near each other, the communication delay can be assumed to be bounded, that is, $0 \leqslant \tau(t) \leqslant \tau_{\max}$.

To verify the effectiveness of the consensus algorithm in this section, the following simulation experiments were conducted. Within the merging area, the composition comprises two vehicles on the on-ramp and seven on the mainline, constituting nine vehicles in close proximity. By employing the multi-agent consensus algorithm, these vehicles effectively achieved a unanimous consensus pertaining to their position, speed, and acceleration dynamics throughout the merging procedure. This collaborative effort guaranteed the maintenance of a secure and appropriate merging distance for all vehicles involved. The results of the consensus algorithm are illustrated in Figs. 3–5.

4.2 Driving styles

Numerous factors, including age, sex, personality traits, and driving experience, contribute to the development of personalized driving characteristics exhibited by individual drivers. Consequently, accurately predicting the intentions of HVs using a standardized merging motion model presents considerable challenges. It becomes evident that defining real-time driving expectations and requirements necessitates the consideration of these personalized driving behavior characteristics. Furthermore, ensuring the establishment of a safe merging gap is a formidable task without considering personalized interaction dynamics with surrounding vehicles, which has profound implications for driving safety.

The maximum acceleration constraint prescribed by the vehicle speed guidance model was based on the average acceptance levels exhibited by human drivers. However, it is crucial to recognize that different drivers possess unique driving traits. When the speed guidance curve

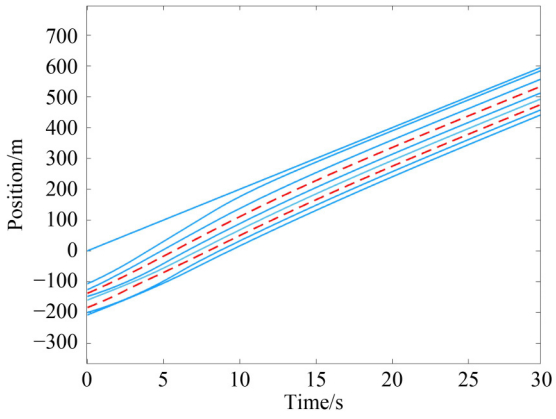

Fig. 3 The position of the 9 vehicles at merging area.

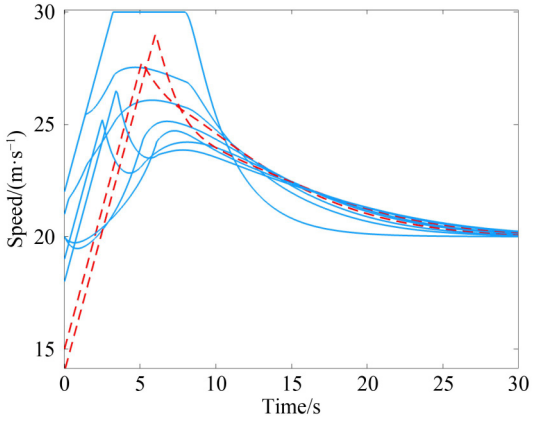

Fig. 4 The speed of the 9 vehicles at merging area.

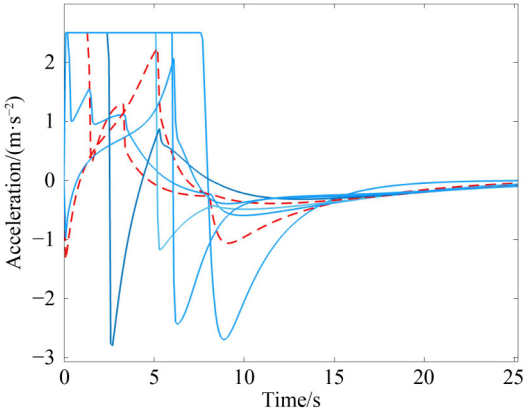

Fig. 5 The acceleration of the 9 vehicles at merging area.

surpasses a driver's acceptance threshold, it introduces discomfort and the potential for loss of effectiveness. Additionally, the distance constraint inherent in the vehicle speed guidance model results in a speed guide curve that assumes precise adherence by the vehicle, which may not align with the preferences of drivers who exhibit strong driving skills and prefer rapid merging. In cases where the control center guides autonomous driving, the vehicle's behavior is fixed to follow the speed guide curve irrespective of the driver's individual preferences.

A driver's distinctive driving style exerts a discernible influence on vehicle speed guidance, manifesting as variability in driver classifications (ranging from aggressive to moderate or conservative) and the stability of their driving behavior. To enhance the adaptability of the vehicle speed guidance system, this study introduced differential constraints for maximum longitudinal acceleration based on distinct driving styles. However, given that the constraint range varies among drivers with varying driving styles, this study employed a stochastic constraint programming method.

First, the driver's acceleration data were segmented into three distinct categories using the fuzzy clustering method, each corresponding to a distinct driving style. Building on statistical samples, the probability distribution governing the maximum longitudinal acceleration was predicted using point-estimation methods. Assuming that the longitudinal maximum acceleration follows a normal distribution, the distribution characteristics are encapsulated by Eq. (18):

$$a_{\max}(m) \sim N(\mu_m, \sigma_m^2), \quad m = 1, 2, 3, \tag{18}$$

where the values of different parameters m indicate different driving styles: $m = 1$ indicates a conservative style, $m = 2$ indicates a moderate style, and $m = 3$ indicates an aggressive style.

The longitudinal maximum acceleration is taken as an example to analyze the probabilistic model modeling process for a conservative driver.

The point estimation method uses sample statistics to estimate the overall parameters. Point estimation aims to estimate the unknown parameter θ based on sample $X = (X_1, X_2, ..., X_n)$. In general, θ is a specific eigenvalue of the population, such as mathematical expectation, variance, and correlation coefficient. The commonly employed point estimation methods include maximum likelihood estimation, moment estimation, and least squares. This section exclusively employs the moment estimation method.

$$\mu_i = E(x^i) = \mu_i(\theta_1, \theta_2, ..., \theta_k), \quad i = 1, 2, ..., k. \tag{19}$$

The moment μ_i of order i of the sample takes the origin moment A_i of order i as the estimation value.

$$\widehat{\mu}_i = A_i = \frac{1}{n}\sum_{j=1}^{n} X_j^k, \quad i = 1, 2, ... \tag{20}$$

Solution:

$$\hat{\theta}_i = \theta_i(X_1, X_2, ..., X_n), \quad i = 1, 2, ..., \tag{21}$$

where the estimation value θ_i is $\hat{\theta}_i$.

Based on the above assumptions, the sample population X_n with the maximum longitudinal acceleration follows a normal distribution, as obtained according to the theory above:

$$\begin{cases} E(X_c)=\mu_1=\dfrac{1}{n_1}\sum\limits_{i-1}^{n_1}X_{ci}=\overline{X}_c \\ E(X_c^2)=\sigma_1^2+\mu_1^2=\dfrac{1}{n_1}\sum\limits_{i-1}^{n_1}X_{ci}^2 \end{cases}. \tag{22}$$

Solved by the above system of equations, μ_1, the moment estimation of σ_1^2, is shown in Eq. (23), where s is sample standard deviation.

$$\begin{cases} \hat{\mu}=\dfrac{1}{n_1}\sum\limits_{i-1}^{n_1}X_{ci}=\overline{X}_c \\ \hat{\sigma}_1^2=\dfrac{1}{n_1}\sum\limits_{i-1}^{n_1}(X_{ci}-\overline{X}_c)^2=\dfrac{n-1}{n}s^2 \end{cases}. \tag{23}$$

5 The closed-loop feedback vehicle speed guidance method

The speed guidance model operates under the assumption that drivers can faithfully adhere to the provided speed profiles. Nonetheless, discrepancies invariably exist between the actual driving speeds and the recommended speeds during real-world driving, subsequently affecting fuel efficiency. It is impractical to retrain all the drivers to conform to the suggested speed profiles. Therefore, the sole viable approach involves adapting the speed profiles to align them with the actual speeds exhibited by human drivers. This adaptation process was encapsulated within the closed-loop feedback vehicle speed guidance system, as shown in Fig. 6.

In this system, the real-time actual driving speed v_{act} of the vehicle is continuously fed back to the speed optimization model as an input parameter. Consequently, the speed optimization model undergoes dynamic adjustments to fine-tune the optimal target speed v_{opt} in a responsive manner, ensuring alignment with actual driving conditions.

5.1 Vehicle speed guidance method based on closed-loop feedback

In Eq. (6), the initial acceleration of the speed optimization model was set to 0. However, during the feedback process, the real vehicle experiences nonzero acceleration, leading to sudden changes in acceleration. Given that the acceleration of the vehicle is not provided as feedback and the acceleration of the speed guidance model remains static, it is necessary to incorporate this acceleration component into the model to ensure its dynamic adjustment. According to Eq. (6), the average target speed v_a has a fixed value. The real vehicle speed v_0 is dynamically updated with the feedback value, and the difference between the target vehicle speed and real vehicle speed, v_d, also changes accordingly. Therefore, v_d can be represented as a function of the acceleration, speed, and time, as shown in Eq. (24), where v_0 is the vehicle speed at the current moment, and the speed optimization profile of Eq. (6) was adjusted to Eq. (25), where a_0 is the acceleration value of the vehicle at the current moment.

$$v_d(t)=\begin{cases} v_a-v_0-a_0t & 0\leqslant t\leqslant\dfrac{\pi}{2\omega} \\ v_a-v_0-a_0\dfrac{\pi}{2\omega} & \dfrac{\pi}{2\omega}\leqslant t\leqslant\dfrac{d_{\text{int}}}{v_a} \end{cases}, \tag{24}$$

$$v_{\text{opt}}(t)=\begin{cases} v_a-(v_a-v_0-a_0t)\cos(\omega t) & 0\leqslant t<\dfrac{\pi}{2\omega} \\ v_a-\left(v_a-v_0-a_0\dfrac{\pi}{2\omega}\right)\dfrac{\omega}{\varphi}\cos\varphi\left(t-\dfrac{\pi}{2\omega}+\dfrac{\pi}{2\varphi}\right) & \dfrac{\pi}{2\omega}\leqslant t<\dfrac{\pi}{2\omega}+\dfrac{\pi}{2\varphi} \\ v_a+\left(v_a-v_0-a_0\dfrac{\pi}{2\omega}\right)\dfrac{\omega}{\varphi} & \dfrac{\pi}{2\omega}+\dfrac{\pi}{2\varphi}\leqslant t<t_f \end{cases}. \tag{25}$$

The constraint conditions are included to get the following Eq. (26):

$$\begin{cases} d_{\text{int}}=\displaystyle\int_0^{\frac{\pi}{2\omega}+\frac{\pi}{2\varphi}}v_a\mathrm{d}t-\int_0^{\frac{\pi}{2\omega}}(v_a-v_0-a_0t)\cos(\omega t)\,\mathrm{d}t \\ \qquad\displaystyle-\int_{\frac{\pi}{2\omega}}^{\frac{\pi}{2\omega}+\frac{\pi}{2\varphi}}\left(v_a-v_0-a_0\frac{\pi}{2\omega}\right)\frac{\omega}{\varphi}\cos\varphi\left(t-\frac{\pi}{2\omega}+\frac{\pi}{2\varphi}\right)\mathrm{d}t \\ \qquad+\left(v_a+\left(v_a-v_0-a_0\dfrac{\pi}{2\omega}\right)\dfrac{\omega}{\varphi}\right)\left(\dfrac{d_{\text{int}}}{v_a}-\dfrac{\pi}{2\omega}-\dfrac{\pi}{2\varphi}\right) \\ |J|=|v_d\omega\varphi|\leqslant 10 \\ |a_{\max}|\leqslant 2.5 \\ \varphi=\max\{\varphi\} \end{cases}. \tag{26}$$

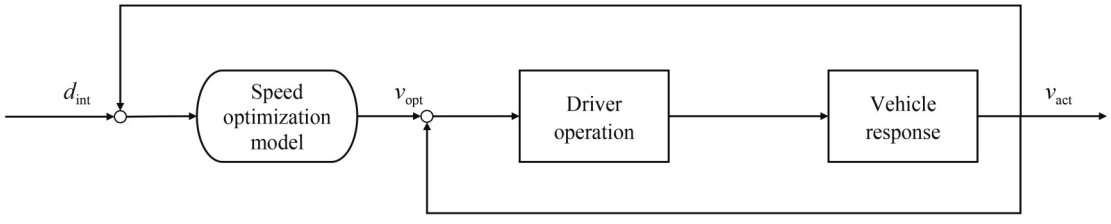

Fig. 6 The closed-loop feedback vehicle speed guidance system.

5.2 Update steps optimization

The efficacy of the closed-loop feedback vehicle speed guidance method was influenced by the reaction time of the driver. If the simulation step length in the speed-guide profile is excessively short, the driver may not be able to make real-time adjustments. Conversely, if the simulation step is excessively long, the vehicle may struggle to accurately track the speed profiles.

To circumvent the issue of high update frequency and ensure that each update provides sufficient time for adjustments, the update step time was established at half of the merging process time. This strategy diminishes the update step length, mitigating the problem of excessively frequent updates. Nevertheless, as the merging process time gradually decreases, the update step time can become exceptionally small. Given that the average driver's reaction time to the guidance speed is approximately 1 s, excessively rapid updates become impractical for human drivers. Consequently, the minimum update step was fixed at 2 s in this study. The guidance speed remained unaltered when the merging process time was less than 2 s. In scenarios where the merging process time is extended to 8 s, the update interval for the speed guidance profile becomes 4 s. The closed-loop feedback vehicle speed guidance method meticulously tracks the speed profiles optimized through a trigonometric function, as previously described.

5.3 Construction of a vehicle speed guidance model based on a chance constrained model

The preceding discussion elucidates the distribution of the maximum longitudinal acceleration for each driver type. By leveraging the statistical model, it becomes feasible to articulate the acceleration distribution corresponding to each driving style, subsequently integrating the distinctive maximum longitudinal acceleration attributes of diverse driving styles into the speed guidance system using a stochastic programming model.

Given the importance of the vehicle speed guidance model in formulating velocity decisions prior to the occurrence of random events, this study opts for the chance-constrained programming model for vehicle speed planning. The chance-constrained programming model belongs to the realm of stochastic parameter-programming techniques. Within this framework, the stochastic programming model contains uncertain elements within both the objective and constraint functions, which are delineated through a probability function. This methodology permits decision making to exhibit a degree of flexibility under constraints, ensuring that the probability of constraint satisfaction surpasses or equals a predefined confidence level α. The formulation is expressed as follows:

$$\begin{cases} \max \bar{f} \ \textit{subject to} \\ P\left\{f(X,\ \varepsilon) \geqslant \bar{f}\right\} \geqslant \beta \\ P\{g_j(X,\ \varepsilon) \leqslant 0,\ j=1,\ 2,\ ...,\ p\} \geqslant \alpha \end{cases}, \tag{27}$$

where $\bar{f}$ is the objective function and $P\{\cdot\}$ represents the probability of event $\{\cdot\}$. α and β are the confidence levels of the constraints and the objective functions, respectively. ε is a random vector representing uncertainty and X is a constraint condition representing certainty. $g_j(X,\ \varepsilon)$ signifies a stochastic constraint function that is applicable to a random vector.

In the speed-guidance model, the acceleration constraint is formulated as a stochastic programming problem. Finally, the constraints of the vehicle speed guidance model considering the randomness of the driver-driving characteristics are as follows:

$$\begin{cases} d_{\text{int}} = \int_0^{\frac{\pi}{2\omega}} (v_a - v_d(t)\cos(\omega t))\,\mathrm{d}t \\ \qquad + \int_{\frac{\pi}{2\omega}}^{\frac{\pi}{2\omega}+\frac{\pi}{2\varphi}} \left(v_a - v_d(t)\frac{\omega}{\varphi}\cos\varphi\left(t - \frac{\pi}{2\omega} + \frac{\pi}{2\varphi}\right)\right)\mathrm{d}t \\ \qquad + \left(v_a + v_d(t)\frac{\omega}{\varphi}\right)\left(\frac{d_{\text{int}}}{v_a} - \frac{\pi}{2\omega} - \frac{\pi}{2\varphi}\right) \\ |J| = |v_d\omega\varphi| \leqslant 10 \\ P\{a_{\max} \leqslant \bar{a}_{\max}\} \geqslant 1-\alpha \\ \varphi = \max\{\varphi\} \end{cases}. \tag{28}$$

In contrast with the foundational speed guidance model, the core objective function remains unaltered in this context. However, notable enhancements were incorporated into the constraint conditions, rendering them uncertainty constraints grounded in chance constraints. Through an analysis of the maximum longitudinal acceleration and probability distributions characterizing drivers with distinct driving styles, the speed guidance model is poised to offer varying maximum guidance accelerations attuned to the individual driving styles under consideration.

Suppose that the random constraint function satisfies the following formula:

$$g(a_{\max},\ \gamma) = a_{\max} - \bar{a}_{\max}, \tag{29}$$

then the constraint of maximum longitudinal acceleration can be transformed into:

$$P\{g(a_{\max},\ \gamma) \leqslant 0\} \geqslant 1-\alpha, \tag{30}$$

where γ represents the randomness of the maximum longitudinal acceleration $a_{\max}$, and $\bar{a}_{\max}$ represents the average of the sample.

Drawing upon the principles of confidence intervals within the framework of the Gaussian probability

distribution, it is possible to establish a confidence interval for the acceleration probability distribution associated with diverse driving styles. Subsequently, this probabilistic constraint can be translated into an inequality constraint, facilitating its incorporation into the speed guidance model.

6 Simulation experiment

6.1 Naturalistic driving experiment

Using a naturalistic driving experimental vehicle, a cohort of 50 participants was enlisted to engage in naturalistic driving experiments conducted on an expressway.

The experimental vehicle was equipped to capture real-time data, including the vehicle's velocity, acceleration, and other pertinent status information. In addition, it can be used to monitor the driving behavior of the operator. The sensor suite employed in the experimental vehicle comprised the following components: RT3000 navigation equipment, camera, Mobileye system, steering wheel sensor, CAN information acquisition system, and two industrial personal computers designated for processing data acquired by the sensor equipment.

This study classified driver styles into three distinct categories: Aggressive, moderate, and conservative. Employing the methodology outlined in Section 4.2, an analysis of the experimental sample data culminates in the determination of the maximum acceleration for each of the three driving styles, and characterizes the distribution attributes of maximum deceleration. Specifically, it encompasses moment estimation techniques to ascertain the mean and variance of these characteristics. The mean and variance estimations of the maximum longitudinal acceleration for conservative drivers are $\hat{\mu} = 2.321$, $\hat{\sigma}_1^2 = 0.03261$; for moderate drivers, $\hat{\mu} = 2.597$, $\hat{\sigma}_1^2 = 0.07412$; and for aggressive drivers, $\hat{\mu} = 2.971$, $\hat{\sigma}_1^2 = 0.09799$.

6.2 Simulation results

Proportional–integral–derivative (PID) control is a widely adopted control technique for various industrial applications. Systems such as Adaptive Cruise Control and standard Cruise Control utilize a PID algorithm to regulate speed tracking. Furthermore, the three control parameters inherent to the PID controller represent the driver's response to speed errors. Adjusting these PID control parameters enables the reflection of different driving behaviors.

The resulting simulation results pertain to the closed-loop feedback guidance model. To underscore the efficacy of the method introduced in this study, the simulation includes vehicle speed guidance based on trigonometric functions for comparative purposes. Figures 7–10 present the simulation outcomes pertaining to the vehicle speed tracking and driving distance. It is important to note that drivers may encounter difficulties in precisely tracking the guidance model speed at high frequencies, and the closed-loop feedback guidance model employs a variable step size. Figures 11–14 illustrate the performance distinctions of the closed-loop feedback guidance model under both fixed and variable step sizes. As previously mentioned, this study utilized PID control in the feedback control system. Adjusting the proportional coefficient K_p of PID can produce different control results. Figures 15–17 depict the velocity error of the closed-loop feedback guidance model under different K_p. Finally, Figs. 18–20 show the results of speed guidance accounting for different driving styles.

Case 1

Initially, feedback updates for speed and acceleration were implemented to enhance the driver adaptability and traffic efficiency. Subsequently, to mitigate the challenge of drivers being unable to track speed updates in a timely manner owing to excessively frequent updates, which could lead to increased fuel consumption from frequent operations, the simulation step size is designated as a variable step size. These two facets serve as the basis for comparison with the vehicle speed guidance model predicted on trigonometric functions, thereby validating its effectiveness, as shown in Figs. 9 and 10.

As depicted in Fig. 10, the closed-loop feedback speed updating algorithm demonstrated the capability to cover a distance exceeding 100 m in 7 s, enabling it to pass through the merging area within this timeframe. Conversely, the trigonometric function speed guidance algorithm falls short of traveling the same distance within 7 s, potentially necessitating a wait for the next opportunity to merge. This observation underscores that the closed-loop feedback-updated speed guidance can reach the merging point ahead of the trigonometric model. In essence, this implies that the closed-loop feedback-updated speed guidance has the potential to enhance traffic efficiency when compared to the trigonometric model.

Case 2

The closed-loop feedback speed guidance system was assessed with fixed step sizes of 2, 3, and 4 s, as indicated in Fig. 14. This analysis was conducted in comparison with the variable step size closed-loop feedback speed guidance system introduced in this study.

In contrast to the trigonometric speed guidance model, the variable step size closed-loop feedback system introduced in this study enhances the adaptability of the system and guarantees uninterrupted passage of vehicles through the merging area within a specified timeframe. As the remaining merging time diminishes continuously, the adaptability superiority of the system becomes more pronounced, mitigating the issue of the dilemma zone to a certain extent, thereby enhancing road traffic safety.

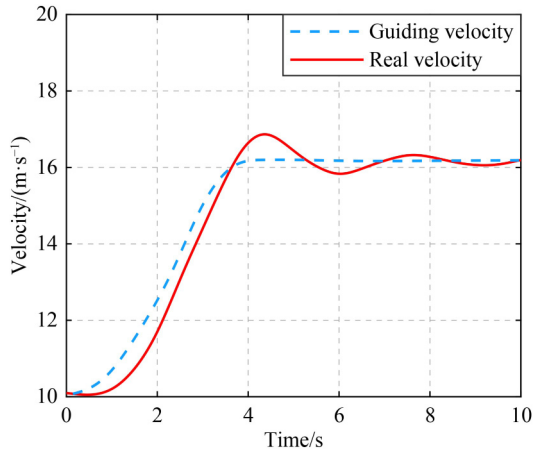

Fig. 7 Speed tracking of the model based on trigonometric function.

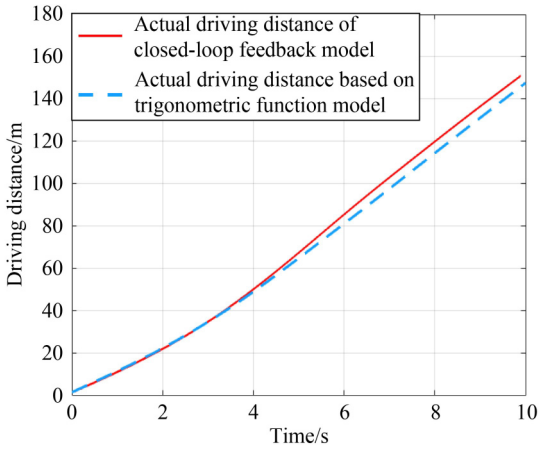

Fig. 9 Driving distance of vehicle tracking under two speed guidances.

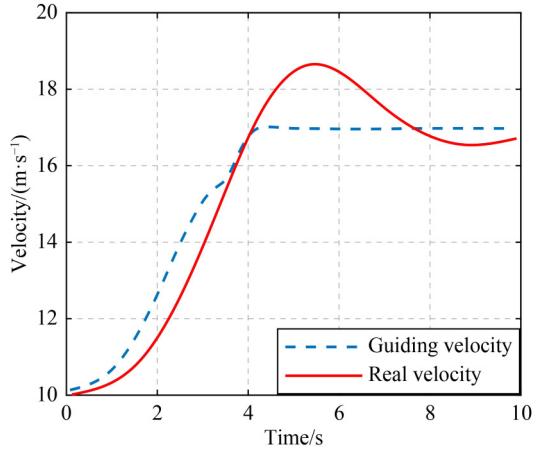

Fig. 8 Variable step size closed-loop feedback speed tracking.

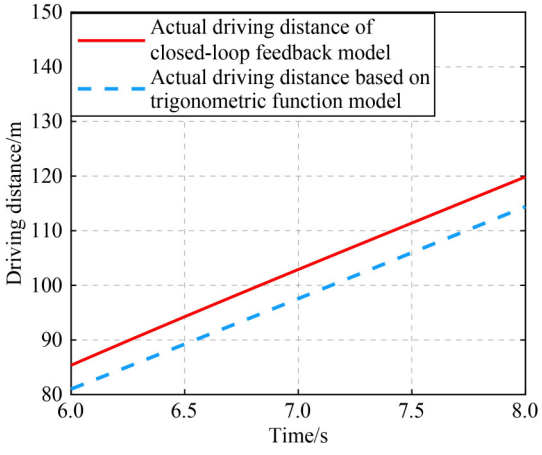

Fig. 10 Local magnification of driving distance.

Case 3

To further analyze the drivers' adaptability, various values of K_p were selected (5, 10, and 20), representing different drivers. The variable step size closed-loop feedback vehicle speed guidance system proposed in this paper was compared to the speeds generated by the trigonometric function vehicle speed guidance model. The results are shown in Figs. 15–17.

Figures 15–17 illustrate the absolute differences between the expected and tracking speeds. The solid line represents the tracking difference of the closed-loop feedback speed guidance algorithm, whereas the dashed line represents the tracking difference of the speed guidance model based on trigonometric functions. It is evident from Figs. 15–17 that the vehicle tracking difference is generally small when using closed-loop feedback speed guidance. The speed tracking error of the closed-loop feedback model gradually decreased, whereas the speed difference amplitude of the trigonometric model increased. Therefore, the variable step size closed-loop feedback speed guidance system exhibits greater adaptability than the trigonometric function speed guidance model. Additionally, as observed in Figs. 15–17, as the value of K_p increases, the speed difference decreases, indicating that different drivers possess varying speed-tracking abilities. Consequently, there is a need to enhance the adaptability of the speed guidance system to drivers by improving the trigonometric function speed guidance model.

Case 4

The speed guidance approach proposed in this paper, which incorporates driving style, primarily addresses two key aspects. First, it models the maximum longitudinal acceleration stochastically to capture variations between drivers with different driving styles. Second, it replaces the distance constraint with the maximum longitudinal driving speed to cater to the diverse requirements of different drivers. The following results show the performance of the closed-loop feedback speed guidance model that integrates driving style compared to a closed-loop feedback speed guidance model that does not consider driving style.

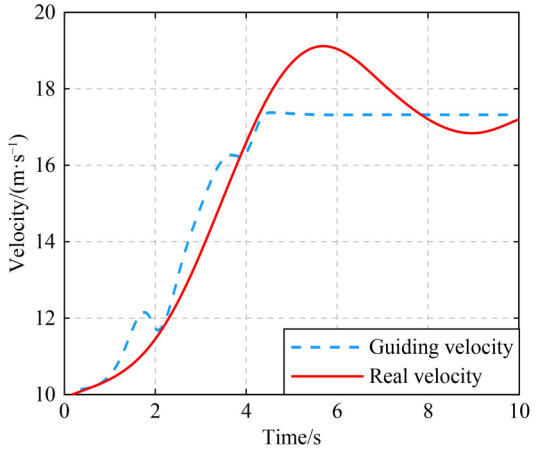

Fig. 11 The curve of closed-loop feedback speed with step size of 2 s.

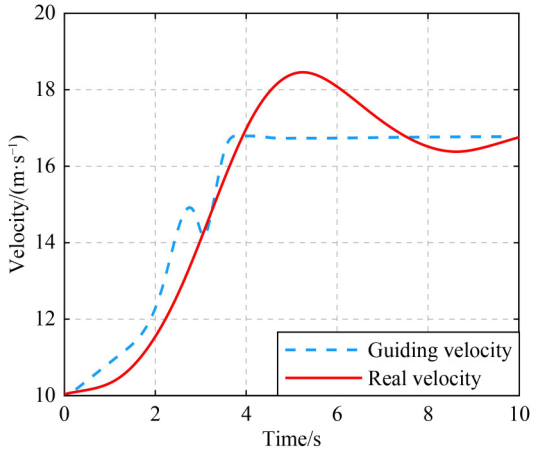

Fig. 12 The curve of closed-loop feedback speed with step size of 3 s.

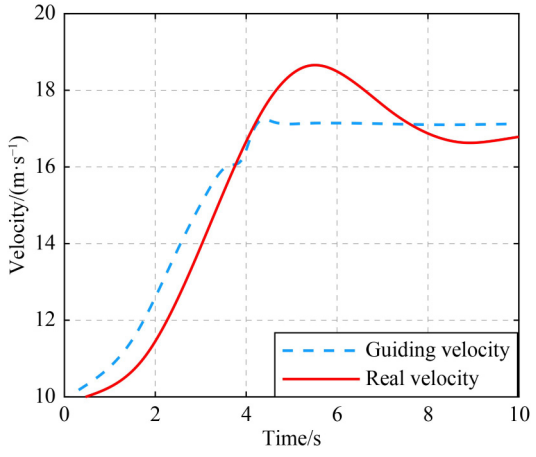

Fig. 13 The curve of closed-loop feedback speed with step size of 4 s.

As shown in Fig. 18, the integration of driving style into speed guidance yields maximum accelerations tailored to various driving styles. Specifically, the aggressive guidance acceleration was the highest, the conservative guidance acceleration was lower than the closed-loop feedback type, and the moderate guidance acceleration fell between the aggressive and conservative types, slightly surpassing the speed guidance model without considering the driving style. In comparison to closed-loop feedback speed guidance that does not account for driving styles, speed guidance systems that consider differences in driving styles can offer customized speed guidance for individual drivers.

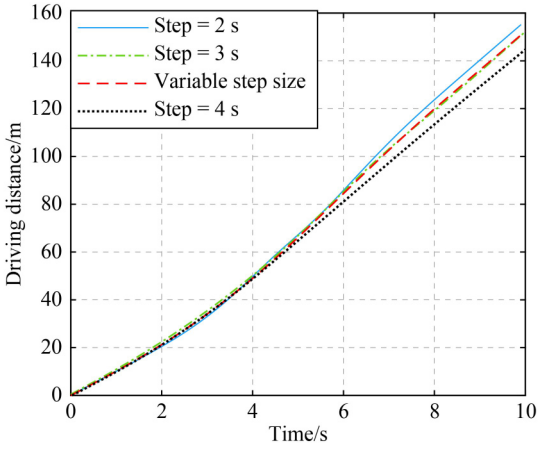

Fig. 14 Driving distance of vehicle tracking under fixed step size and variable step size.

7 Conclusions

This study introduces a dynamic speed guidance method tailored for merging areas on urban expressways. Initially, a multi-agent consensus algorithm was incorporated into the multi-vehicle system, including both the mainline and the on-ramp. This algorithm facilitates the planning of a consistent speed and distance for vehicles, ensuring a harmonized merging process. Furthermore, this study delves into the analysis of driving behavior characteristics exhibited by drivers with distinct styles, leading to more efficient and reliable planned speeds. Additionally, a closed-loop feedback speed guidance method was explored, accounting for the driver's execution rate and enabling dynamic updates of the guided speed. This approach ensures seamless merging of vehicles in merging areas.

Simulation experiments are conducted to validate the adaptability and effectiveness of the proposed method. The results indicate that the enhanced vehicle speed guidance model can significantly improve traffic efficiency, particularly when addressing the dilemma zone in merging areas. Simultaneously, it enhances overall traffic safety, adaptability, and passenger comfort.

Competing Interests The authors declare that they have no competing interests.

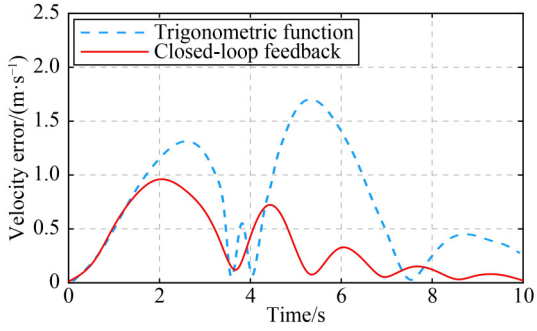

Fig. 15 Speed tracking error when $K_p = 5$.

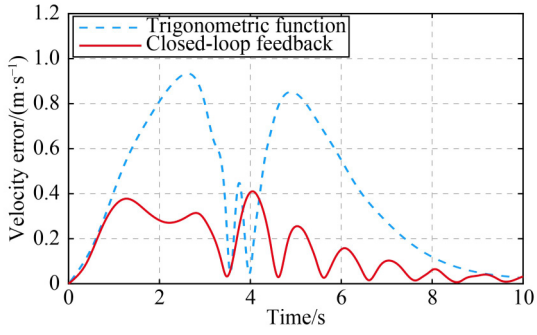

Fig. 16 Speed tracking error when $K_p = 10$.

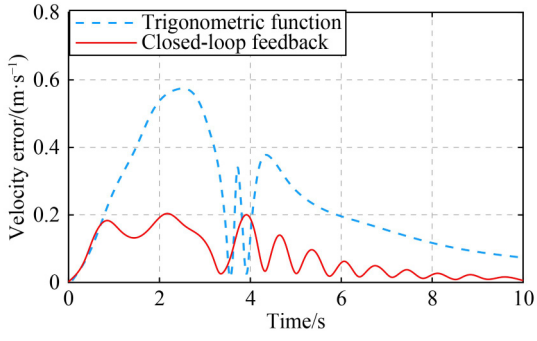

Fig. 17 Speed tracking error when $K_p = 20$.

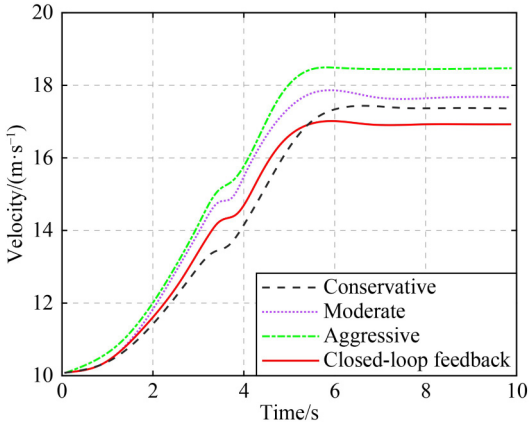

Fig. 18 Speed guidance results of different driving styles.

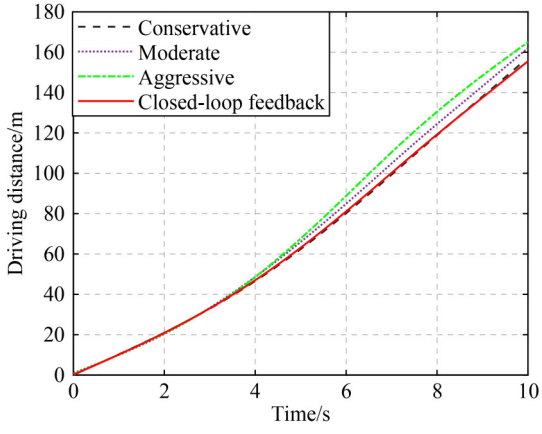

Fig. 19 Driving distance results of different driving styles.

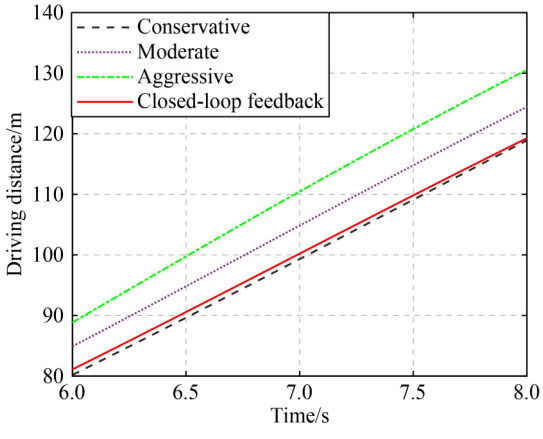

Fig. 20 Local magnification of driving distance.

References

Barth M, Mandava S, Boriboonsomsin K, Xia H (2011). Dynamic ECO-driving for arterial corridors. In: IEEE Forum on Integrated and Sustainable Transportation Systems. Vienna: IEEE, 182–188

Chen W, Liu Y, Yang X, Bai Y, Gao Y, Li P (2015). Platoon-based speed control algorithm for eco-driving at signalized intersection. Transportation Research Record: Journal of the Transportation Research Board, 2489(1): 29–38

Chen X (2019). The development trend and practical innovation of smart cities under the integration of new technologies. Frontiers of Engineering Management, 6(4): 485–502

Chen Z, Liu K, Wang J, Yamamoto T (2022). H-ConvLSTM-based bagging learning approach for ride-hailing demand prediction considering imbalance problems and sparse uncertainty. Transportation Research Part C: Emerging Technologies, 140: 103709

Cheng M, Zhang C, Jin H, Wang Z, Yang X (2022). Adaptive coordinated variable speed limit between highway mainline and on-ramp with deep reinforcement learning. Journal of Advanced Transportation, 2435643

Ci Y, Wu L, Zhao J, Sun Y, Zhang G (2019). V2I-based car-following modeling and simulation of signalized intersection. Physica A, 525: 672–679

Fang S, Yang L, Wang T, Jing S (2020). Trajectory planning method for mixed vehicles considering traffic stability and fuel consumption

at the signalized intersection. Journal of Advanced Transportation, 1456207

Gao Z, Huang H J, Guo J, Yang L, Wu J (2023). Future urban transport management. Frontiers of Engineering Management, 10(3): 534–539

Gipps P G (1986). A model for the structure of lane-changing decisions. Transportation Research Part B: Methodological, 20(5): 403–414

Gong S, Du L (2018). Cooperative platoon control for a mixed traffic flow including human drive vehicles and connected and autonomous vehicles. Transportation Research Part B: Methodological, 116: 25–61

Han J, Sciarretta A, Ojeda L L, de Nunzio G, Thibault L (2018). Safe- and eco-driving control for connected and automated electric vehicles using analytical state-constrained optimal solution. IEEE Transactions on Intelligent Vehicles, 3(2): 163–172

HomChaudhuri B, Vahidi A, Pisu P (2017). Fast model predictive control-based fuel efficient control strategy for a group of connected vehicles in urban road conditions. IEEE Transactions on Control Systems Technology, 25(2): 760–767

Huang K, Yang X, Lu Y, Mi C C, Kondlapudi P (2018). Ecological driving system for connected/automated vehicles using a two-stage control hierarchy. IEEE Transactions on Intelligent Transportation Systems, 19(7): 2373–2384

Karimi M, Roncoli C, Alecsandru C, Papageorgiou M (2020). Cooperative merging control via trajectory optimization in mixed vehicular traffic. Transportation Research Part C: Emerging Technologies, 116: 102663

Kennedy D, Philbin S P (2019). Techno-economic analysis of the adoption of electric vehicles. Frontiers of Engineering Management, 6(4): 538–550

Kherroubi Z E A, Aknine S, Bacha R (2022). Novel decision-making strategy for connected and autonomous vehicles in highway on-ramp merging. IEEE Transactions on Intelligent Transportation Systems, 23(8): 12490–12502

Kim T, Jeong H Y (2014). A novel algorithm for crash detection under general road scenes using crash probabilities and an interactive multiple model particle filter. IEEE Transactions on Intelligent Transportation Systems, 15(6): 2480–2490

Kimura H, Takahashi M, Nishiwaki K, Iezawa M (2022). Decision-making based on reinforcement learning and model predictive control considering space generation for highway on-ramp merging. IFAC-PapersOnLine, 55(27): 241–246

Ladino A, Wang M (2020). A dynamic game formulation for cooperative lane change strategies at highway merges. IFAC-PapersOnLine, 53(2): 15059–15064

Liang X, Guler S I, Gayah V V (2018). Signal timing optimization with connected vehicle technology: Platooning to improve computational efficiency. Transportation Research Record: Journal of the Transportation Research Board, 2672(18): 81–92

Lu X Y, Tan H S, Shladover S E, Hedrick J K (2004). Automated vehicle merging maneuver implementation for AHS. Vehicle System Dynamics, 41(2): 85–107

Marinescu D, Čurn J, Bouroche M, Cahill V (2012). On-ramp traffic merging using cooperative intelligent vehicles: A slot-based approach. In: 15th International IEEE Conference on Intelligent Transportation Systems. Anchorage, AK: IEEE, 900–906

Milanés V, Godoy J, Villagrá J, Pérez J (2011). Automated on-ramp merging system for congested traffic situations. IEEE Transactions on Intelligent Transportation Systems, 12(2): 500–508

Miyajima C, Nishiwaki Y, Ozawa K, Wakita T, Itou K, Takeda K, Itakura F (2007). Driver modeling based on driving behavior and its evaluation in driver identification. Proceedings of the IEEE, 95(2): 427–437

Moridpour S, Sarvi M, Rose G, Mazloumi E (2012). Lane-changing decision model for heavy vehicle drivers. Journal of Intelligent Transport Systems, 16(1): 24–35

Ntousakis I A, Nikolos I K, Papageorgiou M (2016). Optimal vehicle trajectory planning in the context of cooperative merging on highways. Transportation Research Part C: Emerging Technologies, 71: 464–488

Rios-Torres J, Malikopoulos A A (2017). A survey on the coordination of connected and automated vehicles at intersections and merging at highway on-ramps. IEEE Transactions on Intelligent Transportation Systems, 18(5): 1066–1077

Shi Y, Yuan Z, Yu H, Guo Y, Qi Y (2021). A graph-based optimal on-ramp merging of connected vehicles on the highway. Machines, 9(11): 290

Tang T, Huang H, Shang H Y (2017). An extended macro traffic flow model accounting for the driver's bounded rationality and numerical tests. Physica A, 468: 322–333

Uno A, Sakaguchi T, Tsugawa S (1999). A merging control algorithm based on inter-vehicle communication. In: Proceedings of 199 IEEE/IEEJ/JSAI International Conference on Intelligent Transportation Systems. Tokyo: IEEE, 783–787

Wu W, Li P K, Zhang Y (2015). Modelling and simulation of vehicle speed guidance in connected vehicle environment. International Journal of Simulation Modelling, 14: 145–157

Xin Q, Fu R, Yuan W, Liu Q, Yu S (2018). Predictive intelligent driver model for eco-driving using upcoming traffic signal information. Physica A, 508: 806–823

Xu Q, Wang J, Wang B, Yan X (2020). Modeling and simulation of intersection quasi-moving block speed guidance based on connected vehicles. Journal of Intelligent and Connected Vehicles, 3(2): 67–78

Yu C, Feng Y, Liu H X, Ma W, Yang X (2018). Integrated optimization of traffic signals and vehicle trajectories at isolated urban intersections. Transportation Research Part B: Methodological, 112: 89–112

Zhang Y, Ioannou P A (2017). Coordinated variable speed limit, ramp metering and lane change control of highway traffic. IFAC-PapersOnLine, 50(1): 5307–5312

Zhao J, Knoop V L, Wang M (2020). Two-dimensional vehicular movement modelling at intersections based on optimal control. Transportation Research Part B: Methodological, 138: 1–22

Zhao S, Zhang K (2021). Online predictive connected and automated eco-driving on signalized arterials considering traffic control devices and road geometry constraints under uncertain traffic conditions. Transportation Research Part B: Methodological, 145: 80–117

Zhao W, Ngoduy D, Shepherd S, Liu R, Papageorgiou M (2018). A platoon based cooperative eco-driving model for mixed automated and human-driven vehicles at a signalised intersection. Transportation Research Part C: Emerging Technologies, 95: 802–821